In-plane magnetic anisotropies in epitaxial Fe(001) thin films

N. Tournerie,[1] P. Schieffer,[2] B. Lépine,[2] C. Lallaizon,[2] P. Turban,[2] and G. Jézéquel[2]
[1]*Physique de la Matière Condensée, Ecole Polytechnique, CNRS, 91128 Palaiseau, France*
[2]*Equipe de Physique des Surfaces et Interfaces, Institut de Physique de Rennes, UMR 6251, CNRS–Université de Rennes 1, Campus de Beaulieu, Bât 11C, 35042 Rennes Cedex, France*
(Received 4 July 2008; revised manuscript received 8 September 2008; published 1 October 2008)

The role of epitaxial strain for the in-plane magnetic anisotropies is studied for epitaxial Fe(001) thin films (0.9–60 nm) deposited by molecular-beam epitaxy at room temperature on $Al_{0.48}In_{0.52}As(001)$ layers. The correlation between structural and magnetic properties has been investigated using *ex situ* x-ray diffraction (XRD) experiments and magneto-optical Kerr effect (MOKE) measurements. Fe grows in a body-centered-cubic (bcc) structure with epitaxial relationship $Fe(001)\langle 100\rangle \| Al_{0.48}In_{0.52}As(001)\langle 100\rangle$. The mismatch in lattice parameter between pure Fe and $Al_{0.48}In_{0.52}As$ is of 2.3% and the iron films are under an in-plane tensile biaxial strain. The films remain pseudomorphous up to 4.4 nm and then progressively relax when increasing the Fe coverage. All the Fe layers are ferromagnetic at room temperature and show an in-plane magnetization with a fourfold anisotropy (with $\langle 100\rangle$ directions as easy axes) superimposed to a twofold anisotropy (with [110] direction as easy axis) which probably originates from anisotropic bonding at the $Fe/Al_{0.48}In_{0.52}As$ interface. The fourth-order anisotropy constant of the magnetic films shows nonmonotonous changes with Fe coverage. We show that this unusual evolution can be reproduced within the Néel's pair model in which we have considered high-order Néel parameters and included the strain and interface alloying effects. From our analysis we find that this behavior is due mainly to the in-plane strain effect in the films through the bulk magnetoelastic coupling and a fourfold surface anisotropy term whose strength decreases with the film thickness. This surface magnetic anisotropy induced by the broken symmetry at the interfaces favors the $\langle 110\rangle$ directions as easy axis while the bulk magnetoelastic anisotropy induced by an in-plane tensile biaxial strain favors the $\langle 100\rangle$ directions as easy axis. We find that the surface magnetoelastic anisotropy energy contribution to the in-plane magnetic anisotropy energy is much smaller than the other contributions.

DOI: 10.1103/PhysRevB.78.134401 PACS number(s): 75.30.Gw, 75.70.Cn, 78.20.Ls

I. INTRODUCTION

The origin of magnetic anisotropy in epitaxial ultrathin magnetic films is a topic of current interest.[1,2] The shape anisotropy (that generally favors in-plane magnetization) and magnetocrystalline anisotropy usually dominate the magnetic anisotropies of ultrathin films. Besides, the stress effects on thin magnetic films induced by lattice mismatch between film and substrate can also strongly influence the magnetic anisotropy through the magnetoelastic coupling.[3–5] While most attention has been given during the last years to magnetic films exhibiting a preference for out-of-plane magnetization because of the great technological importance of their applications in magnetic storage domain, relatively little is known about in-plane cubic magnetic anisotropy for magnetic thin films (the fourfold contributions are often 1 order of magnitude lower compared to twofold contributions). Yet the understanding of the cubic magnetic anisotropy properties in thin films is essential for the development of magnetic devices.

Only very few groups are experimentally investigating specifically the effects of in-plane strains on the in-plane fourfold magnetic anisotropy in (001) magnetic layers. The systems studied include Fe/V(001) superlattices[6] and body-centered-cubic (bcc) thin films of Fe grown on Si(001) (Ref. 7) and $Al_{0.48}In_{0.52}As(001)$.[8] In these works it was demonstrated by means of the Néel's pair model[9] and from first-principles calculations that an in-plane isotropic biaxial tensile (compressive) strain in bcc iron films tends to enhance (reduce) the volume fourth-order anisotropy constant with respect to that of bulk Fe.[6–8] Even if the influence of the strain effects on the in-plane magnetic anisotropy properties is qualitatively well explained in the bulk of Fe films, the quantitative description of the volume magnetoelastic coupling is not really satisfactory. Besides, the surface and interface magnetoelastic coupling effects of films are still not properly understood.

The purpose of the present study is to determine the origins of the in-plane fourfold magnetic anisotropy for epitaxially strained films of (001)-oriented bcc Fe films on $Al_{0.48}In_{0.52}As(001)$ surfaces. Fe grows epitaxially on $Al_{0.48}In_{0.52}As(001)$ with a cube-on-cube orientation. The mismatch between the lattice parameter of Fe ($a_{Fe}=0.28664$ nm) and the half lattice parameter of $Al_{0.48}In_{0.52}As$ or InP ($a_{InP}/2=0.2935$ nm) is of 2.3%. We have investigated the correlation between structural and magnetic anisotropy properties of the iron thin films using x-ray diffraction (XRD) and magneto-optical Kerr effect (MOKE) experiments combined with scanning tunneling microscopy (STM) experiments. As there are many successful developments and applications of the Néel's pair model[9–15] to analyze the magnetic anisotropy of thin films and multilayers, we have analyzed our experimental data within this model.

As observed by photoemission in a previous study,[16] in the early stage of the iron growth an interdiffusion process takes place between Fe and $Al_{0.48}In_{0.52}As$ and a bcc Fe-based substitutional alloy confined to several atomic planes is formed. In particular there is an In atomic concentration pro-

file above the interface that causes a gradient in the interplanar distance through the film thickness. Hence, we have included this distribution of the lattice strain in the pair model. This allows us to explain qualitatively and quantitatively the thickness dependence of the in-plane fourth-order anisotropy constant of the magnetic films. We demonstrate here in particular that the dominant energy terms that drive the change of the anisotropy constant with the iron thickness are the surface magnetocrystalline anisotropy term and the bulk magnetoelastic coupling term; the strength of the surface magnetoelastic energy is much smaller than the other magnetic anisotropy energies.

II. EXPERIMENT

InP(001) epiready wafers were prepared by thermally removing the oxide under As_4 flux. 9 nm thick $Al_{0.48}In_{0.52}As(001)$ layers were grown by molecular-beam epitaxy at a temperature of 400 °C on 400 nm $Ga_{0.47}In_{0.53}As(001)$ buffer layers lattice-matched to InP(001). The layers were not intentionally doped. The films were protected by a 1 μm amorphous As capping layer and then transferred into a second ultrahigh vacuum (UHV) chamber for Fe deposition. XRD experiments carried out to control the composition of $Al_{0.48}In_{0.52}As(001)$ and $Ga_{0.47}In_{0.53}As(001)$ layers revealed a lattice mismatch lower than 5×10^{-4}. In a second UHV chamber, the As capping layers were removed by thermal desorption at 450 °C. Well-ordered mixed (2×4) and (4×2) reconstructed surfaces were obtained on $Al_{0.48}In_{0.52}As$. Those desorption conditions, controlled using STM measurements, were chosen to achieve both reproducibility and optimal surface organization. Step patterned Fe layers (with the width of the steps between 1.4 and 3 mm) were deposited below 4×10^{-10} mbar from an effusion cell and on substrates maintained at room temperature (RT). The Fe evaporation rate was controlled by a quartz microbalance and the accuracy of the thickness was estimated to be 10%. After Fe deposition the samples were capped with a 2.5 nm thick Au layer to prevent later oxidation. The strain state of the step patterned Fe layers with thicknesses above 4 nm was studied by XRD on a four-circle texture diffractometer (Bruker D8 Discover) using Cu K_{a1} radiation. Conventional *ex situ* MOKE experiments were performed in the longitudinal geometry with a photoelastic modulator vibrating at 50 kHz and a He-Ne laser (λ =633 nm) emitting *s*-polarized light. The Kerr signal (detected at the frequency of 100 kHz), proportional to the magneto-optical Kerr rotation, was measured with an incident angle of the light of 45° and with a spot size of the beam of 0.5 mm.

III. RESULTS AND DISCUSSION

A. XRD measurements

XRD data show that Fe grows in a bcc structure on $Al_{0.48}In_{0.52}As$, with the epitaxial relationship $Fe(001)\langle100\rangle \| Al_{0.48}In_{0.52}As(001)\langle100\rangle$ and a good crystalline quality. The STM images indicate that the growth mode and the surface morphology of iron films are similar to what

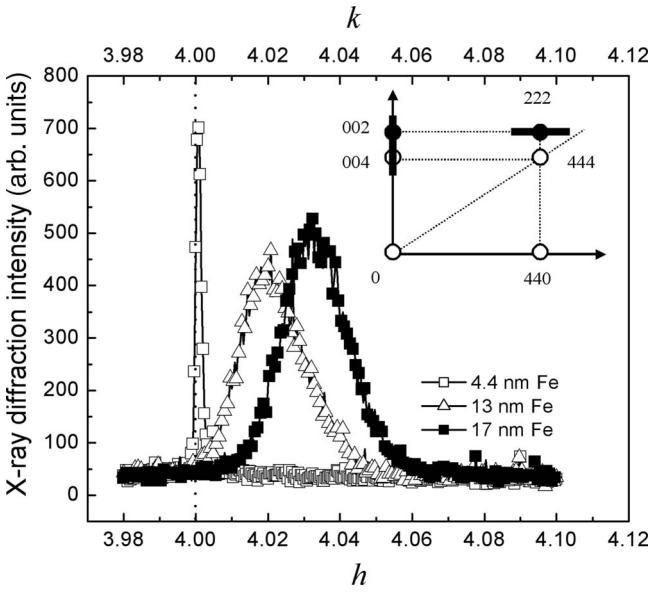

FIG. 1. X-ray diffraction intensity for *hk*-scans (with $h=k$) around the 222 Fe reflection for 4.4, 13, and 17 nm of Fe deposited on $Al_{0.48}In_{0.52}As(001)$ surface at room temperature. The h or k values are the Miller indexes referred to the InP substrate (or $Al_{0.48}In_{0.52}As$ layer). The inset shows the geometrical conditions for the reciprocal space scanning. The (hkl) reciprocal lattice nodes are represented as closed circles for the iron and as open circles for the substrate. To make the figure clearer, not all nodes are represented. Thick lines are for the *l*-scan and *hk*-scan around the Fe 002 and 222 reflections, respectively.

is observed for the Fe layers deposited on GaAs(001) surfaces. The Fe lattice parameters perpendicular ($a_\perp$) and parallel ($a_\parallel$) to the surface were determined by using XRD experiments and scanning the reciprocal lattice as shown in the inset of Fig. 1. From a *l*-scan around the 002 node of Fe reciprocal lattice (θ-2θ symmetrical geometry) and from the l coordinate of the centroid of the diffraction peak, we have determined the d_{002} distance and deduced $a_\perp=2d_{002}$. From this l coordinate, we have made a *hk*-scan (with $h=k$) around the Fe 222 node (ω-2θ asymmetrical geometry) in order to obtain the d_{220} distance and calculated $a_\parallel=2\sqrt{2}d_{220}$. The h or k values are the Miller indexes referred to the InP substrate (or $Al_{0.48}In_{0.52}As$ layer). Figure 1 shows *hk*-scans for 4.4, 13 and 17 nm Fe layers. For the 4.4 nm layer, we clearly see that the Fe 222 reflection is very close to the $h=k=4$ value corresponding to the substrate 444 reflection. This shows that the Fe layer is pseudomorphic with a good crystalline quality as evidenced by the sharpness of the XRD peak (only three times wider than the substrate 444 one, which corresponds to in-plane coherent domain sizes of about 380 nm). For thicker Fe layers, the Fe 222 reflection shifts toward higher values of h (or k) and the XRD peaks width increases (six to ten times depending on films thickness) indicating that stress relaxation takes place within the iron films.

Figure 2 shows the evolution of the in-plane $a_\parallel$ and out-of-plane $a_\perp$ lattice parameters versus Fe thickness. As previously observed, for coverage below 4.4 nm, the iron films are pseudomorphic with the semiconductor surface ($a_\parallel \approx a_{InP}/2$). The same conclusion was drawn from the analysis of reflec-

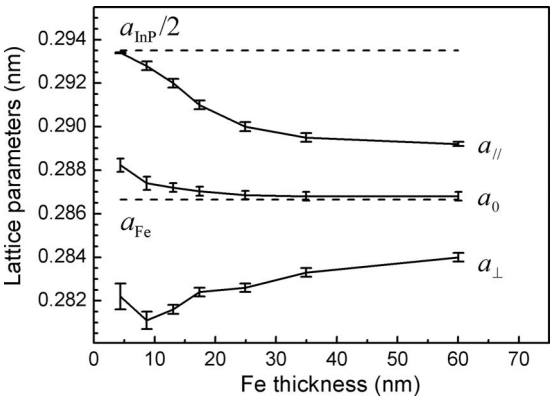

FIG. 2. Plot of in-plane lattice parameter $a_\parallel$ and out-of-plane lattice parameter $a_\perp$ deduced from the XRD measurements as a function of the iron thickness. The stress-free lattice parameter a_0 deduced from the lattice parameters $a_\parallel$ and $a_\perp$ and through the linear elasticity theory using Eq. (1) is also plotted. The lattice parameter of Fe (0.28664 nm) and the half lattice parameter of InP (0.2935 nm) are also represented.

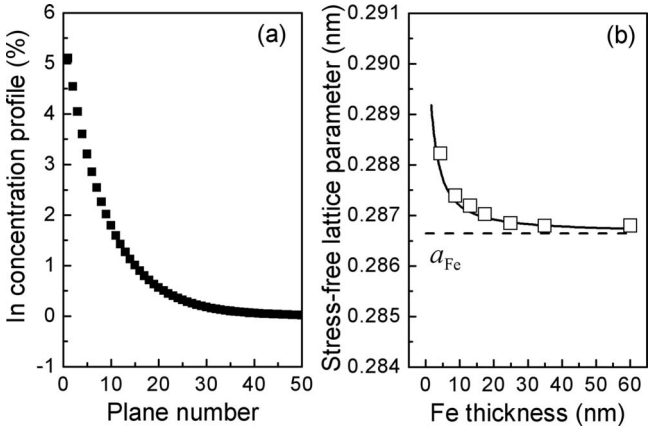

FIG. 3. (a) Model for the indium atomic concentration profile through the Fe film thickness deduced from x-ray photoemission spectroscopy and photoelectron diffraction measurements. (b) Open symbols: evolution of stress-free lattice parameter a_0 deduced from XRD measurements. Continuous line: mean lattice parameter $\langle a_0 \rangle$ determined through the Vegard's law using the In concentration profile given in Fig. 3(a). The bcc In lattice parameter value was assumed to be 0.37 nm (Ref. 21). Note the remarkable agreement between the two curves.

tion high-energy electron diffraction patterns. Above this coverage, a plastic strain relaxation takes place (for example by a progressive introduction of misfit dislocations) and the in-plane lattice parameter decreases from 0.2934 nm at 4.4 nm to 0.2892 nm at 60 nm. The out-of-plane lattice parameter also evolves with the iron coverage and increases from 0.2811 to 0.2840 nm for Fe coverage varying between 8.7 to 60 nm. The marked difference between $a_\perp$ and $a_\parallel$ parameter values demonstrates that the iron lattice undergoes a strong tetragonal distortion which is induced by the in-plane lattice biaxial strain imposed in Fe by the semiconductor layer.

To obtain further information on the in-plane and out-of-plane strain evolution of the Fe lattice as a function of Fe thickness we have calculated the stress-free lattice parameter (a_0) of iron. The a_0 parameter was deduced from $a_\perp$ and $a_\parallel$ parameters in the linear elasticity theory using the following relation:

$$a_0 = \frac{C_{11}a_\perp + 2C_{12}a_\parallel}{C_{11} + 2C_{12}}, \tag{1}$$

with C_{ij} are elastic stiffness constants of bulk bcc Fe: C_{11} =231 GPa and C_{12}=135 GPa.[17]

In Fig. 2 one can see that for a Fe film 4.4 nm thick the a_0 parameter is expanded by 0.6% with respect to the bulk value. Then, as the thickness increases, the a_0 parameter progressively decreases and at 25 nm approaches the bcc bulk value. This expansion of stress-free lattice parameter can be attributed to an interface alloying effect during the $Fe/Al_{0.48}In_{0.52}As$ interface formation and in particular to the presence of indium atoms in the Fe layer. As described in Ref. 16, in the early stage of the iron growth an interdiffusion process takes place between Fe and $Al_{0.48}In_{0.52}As$. A bcc Fe-based substitutional alloy confined to about five atomic planes above the $Fe/Al_{0.48}In_{0.52}As$ interface and containing 15%–20% of foreign species (with similar concentrations for Al, As, and In atoms) is formed during the first five monolayers (0.7 nm) of Fe deposition. This interfacial layer is then buried under a bcc Fe layer on which a fraction of monolayer of As and In atoms float. Some In atoms floating at the surface are progressively trapped in this Fe layer in substitutional sites[18] during the iron growth. Figure 3(a) shows the modeled In atomic concentration (relative to that of iron) profile that we have determined for coverage higher than 1.5 nm from a semiquantitative analysis of x-ray photoemission spectroscopy and x-ray photoelectron diffraction data (results not shown). We have assumed that the In atomic concentration profile drops exponentially as in Ref. 19 and can be written as $C_{In,j}=C_{In,1}\exp(-(j-1)/\lambda)$. j is the Fe plane number (j=1 correspond to the first Fe plane above the $Fe/Al_{0.48}In_{0.52}As$ interface) and the parameter λ is a characteristic decay length.[18] We have found $C_{In,1}$=5.1% and λ =8.6 planes. In our model we consider that for Fe coverage higher than 1.5 nm an In atom trapped into the iron layer does not diffuse and that the overlayer is a uniform slab. Some details about the analysis of x-ray photoelectron diffraction data can be found in Refs. 18 and 20.

Taking into account this In concentration profile, neglecting the presence of As and Al atoms in the iron layer, and omitting surface and interface contributions we have determined the mean lattice parameter $\langle a_0 \rangle$ through the Vegard's law with a bcc In lattice parameter value (a_{In}) of 0.37 nm.[21] Note that this lattice parameter is much higher than that of iron. In Fig. 3(b), $\langle a_0 \rangle$ is plotted and compared to the stress-free lattice parameter a_0 deduced before as a function of iron thickness (t_{Fe}). One can see that $\langle a_0 \rangle$ evolves in the same manner as a_0. We have thus to conclude that the increase in stress-free lattice parameter in Fig. 2 for the thinnest coverage is mainly caused by the incorporation of In atoms in the iron overlayer. Besides, we expect that the incorporation of Al and As atoms in the iron layer also induces an increase in the a_0 parameter.[22,23] However, their atomic volume is much weaker than that of In atoms, and we have therefore ne-

glected their presence in our calculations. For the thickest films (>25 nm), as the contribution of the interface alloy is inversely proportional to the Fe thickness, the a_0 parameter value tends toward that of bulk iron.

Obviously, the shape of the In concentration profile causes a gradient in the interplanar distance. $d_{\perp,j}$ is defined as the distance between the plane numbers $j+1$ and j and in the pseudomorphic regime it is easy to calculate $d_{\perp,j}$ through the linear elastic theory using the following relation:

$$d_{\perp,j} = -\frac{C_{12}}{2C_{11}} a_{\mathrm{InP}} + [a_{\mathrm{Fe}}(1 - C_{\mathrm{In},j}) + a_{\mathrm{In}} C_{\mathrm{In},j}] \frac{2C_{12} + C_{11}}{2C_{11}}. \tag{2}$$

Then, beyond 4.4 nm a strain relaxation appears probably through the formation of misfit dislocations at the interface. However, at this stage we do not have enough information on these mechanisms to obtain the distribution of in-plane lattice parameter of the films. Hence, to calculate the interplanar distance through the film thickness, we will assume for simplicity that the in-plane lattice parameter is homogeneous across the films.

B. MOKE measurements

The MOKE measurements show that all films are ferromagnetic at room temperature with an in-plane magnetic anisotropy. We can note that there is no evidence of out-of-plane magnetization when the external magnetic field is applied in the film's plane. Along the hard axis (HA) the saturation magnetization M_S is reached for a magnetic field H value lower than 100 kA/m. The hysteretic loops $m_L(H)$ ($m_L = M_L/M_S$ is the longitudinal reduced magnetization and M_L the sample magnetization component along the axis of the applied field) obtained with the magnetic field aligned with the substrate directions [1–10] [110], and [100] show that fourfold and twofold (uniaxial) in-plane anisotropies with their easy axes (EA), respectively, along ⟨100⟩ and [110] directions contribute to the magnetic anisotropy. For the thicker Fe films we observe mainly a fourfold magnetic anisotropy with EA along ⟨100⟩, similar to bulk Fe. When decreasing the Fe coverage, the uniaxial magnetic anisotropy (UMA) progressively increases and becomes dominant below 2 nm. This behavior is analogous to the one observed in the Fe/GaAs system.[24,25]

Let us now concentrate on the values of the in-plane uniaxial and fourth-order anisotropy constants of the films K_U and K_4, respectively. These constants are deduced from the shape of the magnetization loops obtained along the HA, i.e., [1–10], substrate direction. In this case, as long as the loops are continuous and without hysteretic effects, the magnetization reversibly rotates while sweeping the magnetic field. Then, as described by Dumm *et al.*,[26] the $H(m_L)$ curve taken from experimental data can be fitted by an analytical expression obtained by minimizing the magnetic energy density including the Zeeman energy. Without any applied magnetic field the angular dependence of this energy density can be expanded for an in-plane magnetization as

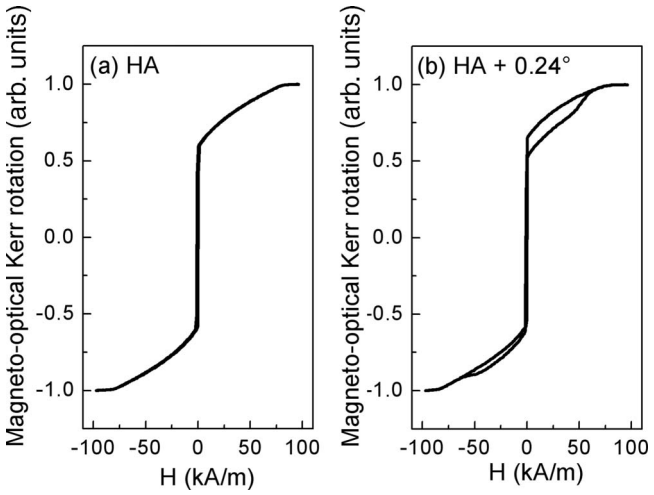

FIG. 4. Hysteresis cycles for 3.8 nm Fe. (a) Following the hard axis [1–10] and (b) with a misalignment of 0.24° between the applied magnetic field and the hard axis.

$$W_M = K_U \sin^2\left(\theta - \frac{\pi}{4}\right) + \frac{1}{4} K_4 \sin^2(2\theta), \tag{3}$$

where θ is the angle between the magnetization and the [100] direction. The value of K_4 is 48 $\mathrm{kJ/m^3}$ for bulk iron at room temperature. The $H(m_L)$ expression can be written as[26]

$$H = \frac{K_4}{\mu_0 M_S}(\alpha + 2m_L^2 - 1)2m_L, \tag{4}$$

where α is the ratio K_U/K_4. Such an analysis yields accurate values of K_U and K_4 if M_S is known. We have used this method to determine the magnetic anisotropy constants on the whole range of Fe coverage. Our magnetization loops are recorded with the magnetic field applied very close to the [1–10] HA. We assume that the reversal of magnetization proceeds by a reversible rotation mechanism except when the loops show irreversible jumps. This approximation will be discussed in more detail later. For example we present in Fig. 4(a) a hysteresis loop recorded with the applied field aligned with the HA with an accuracy better than 0.01°. This magnetization curve perfectly follows the sweeping field reversibly on an extended field range. Hence, the method described above is applicable in this field range. The $H(m_L)$ loops show also an irreversible jump as the field reverses ($H \approx 0.6$ kA/m). For the Fe/GaAs system, Daboo *et al.*[27] demonstrated that this switching corresponds to an irreversible jump of the magnetization over the [110] hard-easy axis. A similar behavior is expected here.

Note that a slight misalignment (≈0.2°) between the applied field and the HA results in a noncentrosymmetrical loop with the clear evidence of two-jump switching processes (at $H \approx 0.6$ and 50 kA/m) while the field reverses [see Fig. 4(b)]. As a result the shape of the $H(m_L)$ curves is not suitable to allow an extraction of the anisotropy constants using our fitting procedure. This asymmetry, often observed in the hysteresis loops measured by MOKE in longitudinal geometry,[28–31] is due to second-order (or quadratic) magneto-optic effects whose amplitude and sign depend on the orien-

tation between the ferromagnetic crystal axes and the magnetization direction.[32] For cubic crystals (001), with an oblique incidence and an in-plane magnetization configuration the magneto-optical Kerr rotation (Φ_K) can be expressed as[33]

$$\Phi_K = b_1 m_L + m_L m_T [b_2 + b_3 \cos(4\gamma)] + b_4 (m_L^2 - m_T^2) \sin(4\gamma), \tag{5}$$

where m_T is the transversal reduced magnetization component, γ is the angle between the magnetic field direction and the [100] direction of the cubic crystal and the b_i are constants. The two last terms are responsible for the noncentrosymmetrical shape of hysteresis loops. By choosing $\gamma = n\pi/4$ (with $n=0,+/-1,+/-2,\ldots$) and canceling the transverse magnetization component these quadratic contributions can be eliminated. In fact due to the magnetic domain structure of the epitaxial films the $m_T=0$ condition will be fulfilled (for all the values of the magnetic field) if the applied field orientation is accurately aligned with one of the hard axes of the ferromagnetic cubic crystal. This property, described in Ref. 34 for epitaxial Fe/GaAs(001) thin films, is a consequence of a magnetic domain splitting process arising from local structural inhomogeneities in the Fe film, when the applied field and the hard axes are carefully aligned with an accuracy better than 0.01°. In this case, it was found that domains with opposite sense of rotation develop upon decreasing the applied field from positive saturation. As a consequence, the total sum of the transverse contributions on the whole domain is equal to zero. As the number of magnetic domains probed by MOKE experiments may be large (~500–2000 domains for a laser spot diameter of 500 μm and for an epitaxial Fe layer[34]) the transverse magnetization component obtained by MOKE measurements is canceled for all the values of the magnetic field. In our approach we have recorded a set of hysteresis loops in the longitudinal geometry for each Fe thickness with an angular step of 0.01° around the [1–10] direction that corresponds to $\gamma=-\pi/4$ and selected the loops that show a centrosymmetrical shape and reversible behavior (except for irreversible jumps that can appear for magnetic fields between −2 and 2 kA/m). Our fitting procedure was applied to the $H(m_L)$ curves deduced from these loops and then K_U/M_S and K_4/M_S values were calculated from an average between the values yielded in ascending and descending branches as well as for negative and positive magnetic fields.

It can be noted that the fitting procedure used to determine the magnetic anisotropy constants is normally strictly applicable for monodomain magnetic films showing a uniaxial anisotropy and for measurements carried out with the magnetic field applied along the HA. In this case the magnetic film can be saturated and there is no jump of the magnetization while sweeping the magnetic films, i.e., the magnetization reversal proceeds by a reversible rotation mechanism. As observed by MOKE microscopy[34] for 30 nm thick epitaxial Fe layer on GaAs(001), 1–5 μm wide domains are formed when the applied field is aligned with the HA. While the Fe layer shows an in-plane biaxial anisotropy, the main mechanism observed upon decreasing the applied field from the positive saturation is the continuous rotation of the magnetization in each domain for positive magnetic fields (the same behavior is expected for negative magnetic fields). During this process, the domain walls are nearly immobile. The rotation of the magnetization in each domain appears to be reversible. As the width of the domain walls is much smaller than the mean lateral size of magnetic domains, the inhomogeneities of the magnetization through the domain walls have negligible effects on the amplitude of the MOKE hysteresis loops. The curve-fitting method can therefore be used to determine the in-plane fourth-order anisotropy constants in the Fe film on GaAs(001) in the field range where no magnetization jump appears. As the magnetic and structural properties of the Fe films on GaAs(001) are very similar to those of the Fe films on $Al_{0.48}In_{0.52}As(001)$, we conclude that the fitting procedure is also valid to determine the fourfold magnetic anisotropy constants of Fe films on $Al_{0.48}In_{0.52}As(001)$.

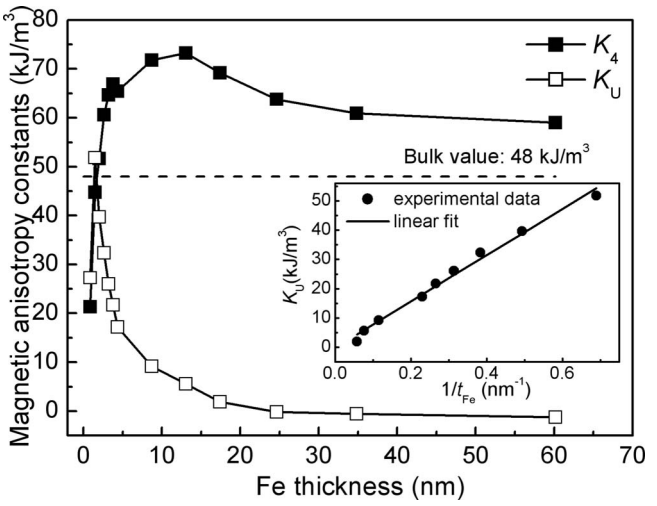

FIG. 5. In-plane magnetic anisotropy constants K_U and K_4 deduced from the MOKE hysteresis loops versus the Fe layer thickness. The inset shows the evolution of the uniaxial constant as a function of the inverse Fe thickness.

In Fig. 5, anisotropy constants K_U and K_4 are plotted versus Fe coverage for thicknesses between 0.9 and 60 nm. To extract these constants we have assumed that the saturation magnetization per unit volume of Fe at room temperature corresponds to the Fe bulk value: $M_S=1.72\times10^6$ A/m. This hypothesis is justified by measurements of the iron magnetization using Brillouin light scattering technique[35] on Fe/GaAs and Fe/InAs systems that demonstrated that above 1.4 nm Fe, the M_S value is very close to that of bulk Fe. Besides, we observe that between 0.9 and 4 nm the magneto-optical Kerr rotation amplitude at saturation is proportional to the Fe coverage. This indicates that the magnetic moment carried by iron atoms does not evolve significantly for Fe films thickness higher than 0.9 nm (due to optical penetration depth, the thickness dependence of the Kerr rotation at saturation does not follow a linear variation above 4 nm).

C. Discussion

The thickness dependence of K_4 can be divided into three regions: an initial linear increase, followed by a weakly

marked peak at 13 nm, and then a progressive decrease. Note that the value at 60 nm is significantly higher than that of bulk iron. The K_U value, comparable with the K_4 value at 1.4 nm, decreases progressively with the film thickness and above 17 nm K_U becomes negligible and Fe films essentially show an in-plane fourfold magnetic anisotropy. This evolution suggests that the uniaxial anisotropy term finds its origin in the interface anisotropy. To demonstrate this, the magnetic anisotropy constant K_U was decomposed into volume (vol) and interface (int) contributions:

$$K_U = K_U^{\mathrm{vol}} + \frac{K_U^{\mathrm{int}}}{t_{\mathrm{Fe}}}. \tag{6}$$

In the inset of Fig. 5, K_U is plotted as a function of inverse Fe thickness between 1.4 and 17 nm. The data are well fitted by a straight line and our analysis yields $K_U^{\mathrm{int}} = (7.9 \pm 0.3) \times 10^{-5}$ J/m^2 and $K_U^{\mathrm{vol}} = (0 \pm 1)$ kJ/m^3. The volume contribution appears insignificant demonstrating that the in-plane UMA has a purely interfacial origin. The interface constant obtained here is of the same sign and order of magnitude than the one measured for the Fe/GaAs(001) system.[24] Our scanning tunneling microscopy experiments (results not shown) performed with uncapped iron films deposited on $Al_{0.48}In_{0.52}As(001)$ show that the surface roughness of Fe films is mainly isotropic. Moreover the in-plane UMA is observed even when the Fe films are pseudomorphous. Therefore, we exclude in-plane shape anisotropy and (surface and volume) magnetoelastic effects as possible explanations of this in-plane UMA. In fact, this anisotropy must be mainly caused by the anisotropic bonding at the $Fe/Al_{0.48}In_{0.52}As$ interfaces. Such an interpretation has already been proposed to explain the interface UMA for Fe/GaAs(001) and Fe/ZnSe systems for which the theoretical calculations reproduced well the experimental findings.[24,36–38] Finally, it can be seen in Fig. 5 that at 0.9 nm the K_U term falls down. As discussed above this is not due to the reduction of M_S, and we explain this drastic change by the fact that the $Fe/Al_{0.48}In_{0.52}As$ interface is probably not completely formed at 0.9 nm.

In Fig. 5, the most remarkable feature is the nonmonotonous thickness dependence of the fourth-order anisotropy constant. Thus, the usual decomposition of the constant under the form

$$K_4 = K_4^{\mathrm{vol}} + \frac{2K_4^{\mathrm{int}}}{t_{\mathrm{Fe}}}, \tag{7}$$

where K_4^{vol} and K_4^{int} are the volume and interface constant contributions to the anisotropy, is not suitable to model our experimental results on the whole range of thickness; i.e., the K_4^{vol} and K_4^{int} constants seem to be dependent on the film thickness (the factor of 2 is present in the relation because the interface contributions are usually assumed to be the same for both surfaces of the film). For the largest thickness of 60 nm, where the interface contributions are negligible, the K_4 value is still 23% larger than the bulk value while the in-plane lattice strain is about 0.9%. Such a change in in-plane fourfold magnetic anisotropy energy with the in-plane biaxial lattice strain has been observed for Fe films on $Al_{0.48}In_{0.52}As(001)$,[8] Si(001),[7] and V(001) (Ref. 6) and interpreted as being the result of a lattice mismatch strain effect through magnetoelastic coupling. To reveal this effect it is necessary, in cubic or tetragonal symmetries, to expand the film magnetoelastic energy density up to the fourth degree in the direction cosines of the magnetization whereas the expansion can be limited to the first order in strains.[10] When the thickness of the film becomes very large, the interface and surface contributions are negligible, and consequently the symmetry of our magnetic layer can be considered as cubic. In this case we can try to estimate the magnetoelastic coupling effect using the angular dependence of the magnetoelastic energy density in (001)-oriented lattice with in-plane magnetization and in-plane isotropic biaxial strain which can be written as

$$W_{\mathrm{me}} = \left[\frac{2}{3}(B^{\alpha,4} - B^{\gamma,4})e_{\parallel} + \frac{1}{3}(B^{\alpha,4} + 2B^{\gamma,4})e_{\perp}\right]\frac{1}{4}\sin^2(2\theta), \tag{8}$$

where $e_{\parallel}(e_{\perp})$ is the in-plane (out-of-plane) strain and $B^{\alpha,4}$ and $B^{\gamma,4}$ are the bulk magnetoelastic coefficients of Fe that are related to the bulk magnetostriction constants $\lambda^{\alpha,4}$ and $\lambda^{\gamma,4}$ by the following relations:[39] $B^{\alpha,4} = -(C_{11} + 2C_{12})\lambda^{\alpha,4}$ and $B^{\gamma,4} = -(C_{11} - C_{12})\lambda^{\gamma,4}$. But these high-order magnetostriction constants are very small and are known only with a large uncertainty. In certain cases the constants measured by two different groups differ even in sign.[40] Hence we conclude that the quantities $\lambda^{\alpha,4}$ and $\lambda^{\gamma,4}$ are not known with sufficient accuracy to allow an estimate of the magnetoelastic coupling effect.

Note that because of the fact that $e_{\parallel}$ is imposed on the films by the substrate, an additional magnetoelastic contribution to the magnetocrystalline anisotropy constant arises from the minimization of the free energy with respect to $e_{\perp}$.[10,41] However, we find that this contribution, often ignored in the literature, is rather small compared to the strength of the magnetocrystalline anisotropy energy and therefore this effect can be neglected.

In order to explain the thickness dependence of K_4 we have then used the Néel's pair model taking the strain effect into account as this was done in Ref. 7. The presence of foreign species located in the substitutional sites of the Fe lattice close to the $Fe/Al_{0.48}In_{0.52}As$ interface as well as the distribution of the in-plane lattice strain through the film thickness will be also considered in the phenomenological model. Within our approach we observe that the change in the fourfold magnetic anisotropy energy with the iron coverage is mainly caused by both the surface magnetic anisotropy due to the broken symmetry at the film surface and the lattice misfit strain effects in the films through the bulk magnetoelastic coupling.

A considerable amount of work has been devoted in the past to the understanding of the surface magnetic anisotropies in magnetic films by means of the Néel's pair interaction model. More specifically the Néel's model has produced good quantitative results for the perpendicular anisotropy for in-plane strained (001)-oriented magnetic epitaxial films of cubic material in which the symmetry breaking at surface/interface as well as the strain effects in bulk induce a second-

order anisotropy.[41] Much less is known about the fourfold magnetic anisotropy in thin magnetic films. This is due to the fact that the cubic magnetocrystalline anisotropy energy is usually of an order of magnitude lower than that of the second order. Recently Bertoncini *et al.*[7] have used the Néel's pair model and considered high-order Néel contributions to establish a relationship between the strain and the K_4 constant of epitaxial Fe layers grown on Si(001). In the present work we have used a similar way in order to analyze our experimental results.

At this stage, let us briefly introduce the Néel's pair model. Néel[9] assumed that the magnetic pair interaction energy between the two atoms depends on the interatomic distance r and the angle (noted Ψ) between the orientation of the magnetic moments and the bond axis. In this model the magnetic anisotropy energy may be expanded as a Legendre polynomial series which takes the form

$$w(r,\Psi) = g_2(r)P_2(\cos\Psi) + g_4(r)P_4(\cos\Psi) + \ldots . \quad (9)$$

Here, $P_n(\cos\Psi)$ terms are the Legendre polynomials of degree n, and $g_i(r)$ are coefficients depending only on the distance between two atoms. The absolute value of the $g_i(r)$ coefficients strongly decreases with increasing the order of the series expansion. Then, considering a strained crystal and introducing the interaction parameters l, m, q and s, the energy becomes

$$w(r_0+\delta r,\Psi) = \left(l + mr_0\frac{\delta r}{r_0}\right)\left(\cos^2\Psi - \frac{1}{3}\right) + \left(q + sr_0\frac{\delta r}{r_0}\right) \times \left(\cos^4\Psi - \frac{6}{7}\cos^2\Psi + \frac{3}{35}\right) + \ldots , \quad (10)$$

where r_0 is the bulk unstrained bond length and δr is the change in bond length after a deformation. As we are interested in the fourfold magnetic anisotropy, only the terms in $\cos^4\Psi$ appearing in the expansion of pair interaction energy are important here and the complete change in $w(r,\Psi)$ induced by strains is given by[7]

$$\delta w^{(4)} = q\,\delta(\cos^4\Psi) + sr_0\frac{\delta r}{r_0}(\cos^4\Psi). \quad (11)$$

We calculate then the angular dependence of the bulk magnetoelastic energy for the film by summing this pair energy over all the pairs of atoms in the crystal. Generally, due to the short range character of pair interactions, this summation is restricted to the nearest neighbor (NN) pairs of atoms. However, in the bcc structures, the bond lengths for the first and second coordination shells are very close, consequently the next-nearest-neighbor (NNN) pair contributions must also be taken into account in the calculation of the interaction energy.[7,12]

Here we consider a (001)-oriented bcc film under an in-plane isotropic biaxial strain ($e_{xx}=e_{yy}=e_{\parallel}$ and $e_{zz}=e_{\perp}$) with the magnetization (assumed uniform over the whole film) lying in the plane of the film. In this case, we find from the Néel's pair model expanded up to first order in strains that the bulk magnetoelastic contribution to the in-plane fourfold magnetic anisotropy may be expressed as a function of the interaction parameters and the strain tensor components in the following way:

$$K_{4,\mathrm{me}}^{\mathrm{vol}} = n\left\{\left[\left(\frac{32}{27}r_1 - 2r_2\right)s + \frac{64}{27}q(r_1)\right]e_{\parallel} + \left[\frac{16}{27}r_1 s - \frac{64}{27}q(r_1)\right]e_{\perp}\right\}, \quad (12)$$

where r_1 (r_2) is the radius of the first (second) neighbor shell and n is the number of sites per unit volume which is considered as constant in the following. A similar relation was found in Refs. 7 and 13.

The surface magnetoelastic anisotropy energy term can be calculated in the same way. There are two interfaces within the thin film, thus the magnetic anisotropy constant of the magnetic film is usually written under the form $K_4 = K_4^{\mathrm{vol}} + 2K_4^{\mathrm{int}}/t_{\mathrm{Fe}}$. Following this formulation, the surface magnetoelastic anisotropy term must be deduced from the difference between the anisotropy energy of surface and bulk atoms. The surface/interface magnetoelastic anisotropy term becomes

$$K_{4,\mathrm{me}}^{\mathrm{int}} = na_{\mathrm{Fe}}\left\{\left[-\frac{8}{27}r_1 s - \frac{16}{27}q(r_1)\right]e_{\parallel} + \left[-\frac{4}{27}r_1 s + \frac{16}{27}q(r_1)\right]e_{\perp}\right\}. \quad (13)$$

For simplicity, the interaction energies between magnetic and nonmagnetic atoms at interfaces were neglected and the NN and NNN Fe-Fe interatomic distances were assumed to be identical to those in the volume. These approximations may appear rather crude however we will see in the following that the surface magnetoelastic anisotropy term is negligible compared with the other magnetic anisotropy terms.

Proceeding in the same manner as before, we have determined the expression of the bulk and interface fourth-order magnetocrystalline anisotropy constants. It can be noted that the interface magnetic anisotropy appears to be weakly sensitive to interface material. Indeed for the Au/Fe/Au(001),[42] Ag/Fe/Ag(001),[43] Au/Fe/GaAs(001),[35] Cu/Fe/GaAs(001),[44] or Au/Fe/ZnSe(001) (Ref. 36) systems the in-plane fourth-order surface anisotropy constant K_4^{int} varies only between -1.8×10^{-5} and -2.6×10^{-5} J/m^2 suggesting that the interface anisotropy originates mainly from the broken symmetry at the interfaces and that the nature of nonmagnetic atoms plays only a secondary role.[15] Hence, we have again neglected, in our calculations, the interaction energies between magnetic and nonmagnetic atoms at interfaces. In agreement with the results of other works,[15] we find that the bulk and surface magnetocrystalline anisotropy constants can be written, respectively, as

$$K_{4,\mathrm{mc}}^{\mathrm{vol}} = n\left[\frac{16}{9}q(r_1) - 2q(r_2)\right] \quad (14)$$

and

$$K_{4,\mathrm{mc}}^{\mathrm{int}} = n a_{\mathrm{Fe}} \left[-\frac{4}{9} q(r_1) \right]. \tag{15}$$

Finally for a homogeneous Fe film, the anisotropy constant K_4 can be decomposed in the following manner:

$$K_4 = K_{4,\mathrm{mc}}^{\mathrm{vol}} + \frac{2K_{4,\mathrm{mc}}^{\mathrm{int}}}{t_{\mathrm{Fe}}} + K_{4,\mathrm{me}}^{\mathrm{vol}} + \frac{2K_{4,\mathrm{me}}^{\mathrm{int}}}{t_{\mathrm{Fe}}}. \tag{16}$$

In order to make a quantitative analysis of the thickness dependence of the fourfold in-plane magnetic anisotropy, we need to know the values of the interaction parameters q and s. In Ref. 7, q and s values were deduced from the fourfold anisotropy energies of bulk Fe and Fe_3Si ordered alloy by means of the Néel's pair model in which the interaction energy relative to the Fe-Si pairs of atoms were neglected, and using the approximation

$$s = \frac{dq}{dr} \approx \frac{q(r_2) - q(r_1)}{r_2 - r_1}. \tag{17}$$

For the pure bcc Fe crystal[7] the interaction energies were estimated to be $nq(r_1) = 8.5 \times 10^4$ J/m^3 and $nq(r_2) = 5.1 \times 10^4$ J/m^3. Using these values, we observe that the Néel's pair model allows predicting correctly the increase in bulk constant for increasing tensile strain. It appears however that the calculated values for K_4 differ significantly from the experimental results. For example the change in the anisotropy constant (as compared to the bulk value) for the largest thickness of 60 nm where $e_{\parallel} = 0.92\%$ is expected to be about +14%, whereas one observes experimentally an increase of about 23%. We conclude that this difference is probably due to the approximate determination of the interaction parameters. It can be noted also that the Fe-Si alloy generally crystallizes with a chemical order. In particular the Fe_3Si compound has a $DO3$-type ordered structure in which the electronic properties are strongly modified as compared to those of pure Fe.[45] For example, there are two different Fe sites on which the atomic magnetic moments are 2.2 and $1.3\mu_B$.[46] Hence we expect that the interaction parameters between Fe-Fe pair of atoms in the Fe_3Si alloys are different from those in pure iron. Consequently we propose here to extract these quantities from our experimental data.

In order to determine the interaction parameter from our data, we have to consider the presence of foreign species located in the substitutional sites of the Fe lattice as well as the distribution of the lattice strain through the film thickness in the pair model. In Sec. III A we have discussed the film inhomogeneity with respect to the chemical environment of the Fe atoms through the film thickness (Fe atomic concentration in the jth plane will be noted $C_{\mathrm{Fe},j}$). A bcc Fe-based substitutional alloy confined only to several atomic planes (about five) is formed above the $Fe/Al_{0.48}In_{0.52}As$ interface. This alloy contains 15%–20% of foreign species (Al, As and In). The presence of foreign atoms causes a modification of the first and second coordination shells around the Fe atoms and consequently we expect the Al, As, or In atoms modify the magnetic anisotropy properties for the lower Fe thicknesses. Besides, we have also shown that the incorporation of In atoms in the Fe lattice tends to increase the stress-free lattice parameter of iron. As the In atomic concentration is not homogeneous through the film thickness, an interplanar distance gradient appears.

To take into account these two effects in the Néel's pair model we have to decompose the in-plane fourth-order anisotropy constant of the magnetic film into a sum of individual plane contributions including the interface contributions under the form

$$K_4 = K_{\mathrm{mc}}^{\mathrm{vol},\Sigma} + K_{\mathrm{me}}^{\mathrm{vol},\Sigma} + K_{\mathrm{mc}}^{\mathrm{int},\Sigma} + K_{\mathrm{me}}^{\mathrm{int},\Sigma}, \tag{18}$$

where

$$K_{\mathrm{mc}}^{\mathrm{vol},\Sigma} = \sum_{j=1}^{N} \frac{1}{N} (K_{4,\mathrm{mc}}^{\mathrm{vol},j}),$$

$$K_{\mathrm{me}}^{\mathrm{vol},\Sigma} = \sum_{j=1}^{N} \frac{1}{N} (K_{4,\mathrm{me}}^{\mathrm{vol},j}),$$

$$K_{\mathrm{mc}}^{\mathrm{int},\Sigma} = \frac{K_{4,\mathrm{mc}}^{\mathrm{int},1} + K_{4,\mathrm{mc}}^{\mathrm{int},N}}{t_{\mathrm{Fe}}},$$

and

$$K_{\mathrm{me}}^{\mathrm{int},\Sigma} = \frac{K_{4,\mathrm{me}}^{\mathrm{int},1} + K_{4,\mathrm{me}}^{\mathrm{int},N}}{t_{\mathrm{Fe}}},$$

where N is the Fe thickness given in monolayers and j is the Fe plane number parallel to the interface ($j=1$ corresponds to the first Fe plane above the interface) and $K_{4,\mathrm{mc}}^{\mathrm{vol},j}$ ($K_{4,\mathrm{me}}^{\mathrm{vol},j}$) is the bulk magnetocrystalline (magnetoelastic) anisotropy term for a homogeneously strained Fe-based crystal in which the interplanar distance would be $d_{\perp,j}$, the Fe atomic concentration would be $C_{\mathrm{Fe},j}$ and the in-plane lattice parameter would be $a_{\parallel}$. The surface (interface) magnetocrystalline anisotropy energy term is $K_{4,\mathrm{mc}}^{\mathrm{int},N}$ ($K_{4,\mathrm{mc}}^{\mathrm{int},1}$) and the surface (interface) magnetoelastic anisotropy energy term is $K_{4,\mathrm{me}}^{\mathrm{int},N}$ ($K_{4,\mathrm{me}}^{\mathrm{int},1}$). The different terms appearing in the expression of K_4 are developed in the Appendix.

The strength of the interaction parameters can be determined from the experimental data for pure bcc Fe and strained bcc Fe(001) films by means of Eqs. (14) and (A1)–(A5). In our model, the interface contributions are not properly taken into account because the interaction energies relative to the interface bonds (Fe-Au and $Fe\text{-}Al_{0.48}In_{0.52}As$) are neglected. Moreover the foreign species (Al, As, and In) concentration profile in the Fe lattice in the first planes above the $Fe/Al_{0.48}In_{0.52}As$ interface is not well known. Therefore, to limit the importance of interface contributions in the determination of the interaction parameters, we have restricted the data analysis to the Fe films with thicknesses between 4.4 and 60 nm. The values for $nq(r_1)$ and $nq(r_2)$ that we have obtained are displayed as a function of Fe thickness in Fig. 6. In the inset are shown the atomic concentration profiles (deduced from photoemission measurements) included into the Néel's pair model to calculate the interaction parameters ($C_{\mathrm{Al},j}$ and $C_{\mathrm{As},j}$ are the atomic concentration profiles for Al and As, respectively). Note that the result of our calculations depends little on the exact shape of the concentration profiles.

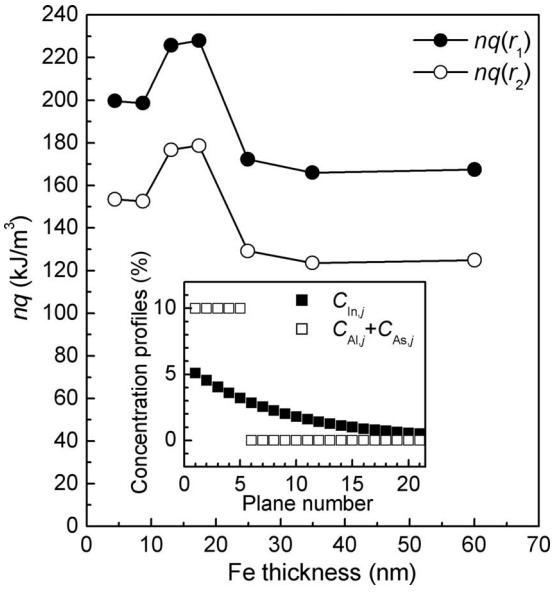

FIG. 6. Evolution of Néel parameters $nq(r_1)$ and $nq(r_2)$ deduced from the K_4 values for bcc Fe and strained bcc Fe(001) films using Eqs. (14) and (A1)–(A5) as a function of the Fe thickness. The inset shows the atomic concentration profiles through the Fe film thickness entered into the Néel's model. $C_{\mathrm{Al},j}$, $C_{\mathrm{As},j}$, and $C_{\mathrm{In},j}$ are atomic concentration profiles for Al, As, and In, respectively.

Whereas we expect that $nq(r_1)$ and $nq(r_2)$ are constant on the whole range of Fe coverage, one can see in Fig. 6 that these parameters slightly vary with the Fe coverage. These fluctuations are about 20% around mean values. Note that a relative error of 3% on the determination of the anisotropy constant K_4 induces a relative error of 15%–25% on the strength of interaction parameters. Other experimental errors appear in our measurements, for example, those concerning the lattice parameter determination which yields a relative error of 5%–7% on the strength of interaction parameters. Hence, we conclude that the variations of the parameters in Fig. 6 most probably originate from experimental errors. Thus in the following, we will use the mean values that are $nq(r_1)=(1.9\pm0.6)\times10^5$ J/m^3 and $nq(r_2)=(1.5\pm0.5)\times10^5$ J/m^3.

In order to analyze the thickness dependence of the in-plane fourfold magnetic anisotropy energy in the Fe films deposited on $Al_{0.48}In_{0.52}As(001)$ surfaces, we have calculated the four terms appearing in Eq. (18) on the whole range of Fe coverage using the relations given in the Appendix with the interaction parameters determined before, the same composition profiles as shown in the inset of Fig. 6, and the in-plane lattice parameters obtained from XRD measurements. By summing these terms we obtain the K_4 curve that is shown (closed circles) in Fig. 7(a). The agreement between the experimental data (continuous line) and the results of calculations is remarkable, demonstrating that, despite approximations, the Néel's pair model is able to correctly reproduce our experimental results on the whole range of Fe coverage. This indicates that our approach is appropriate to perform a quantitative analysis of magnetic anisotropy properties.

Figure 7(b) shows a plot of the four terms appearing in the expression of K_4. The interface magnetoelastic anisotropy term ($K_{\mathrm{me}}^{\mathrm{int},\Sigma}$) is negligible when compared with the other terms. Including the effect of a Fe(001) surface/interface relaxation in the Néel's pair model we find that the $K_{\mathrm{me}}^{\mathrm{int},\Sigma}$ term is always much lower (in absolute value) than the $K_{\mathrm{mc}}^{\mathrm{int},\Sigma}$ term even with surface relaxations of $\pm4\%$.[47] Thus, we conclude that the in-plane surface magnetic anisotropy finds mainly its origin in an anisotropy induced by the broken symmetry at the interfaces.

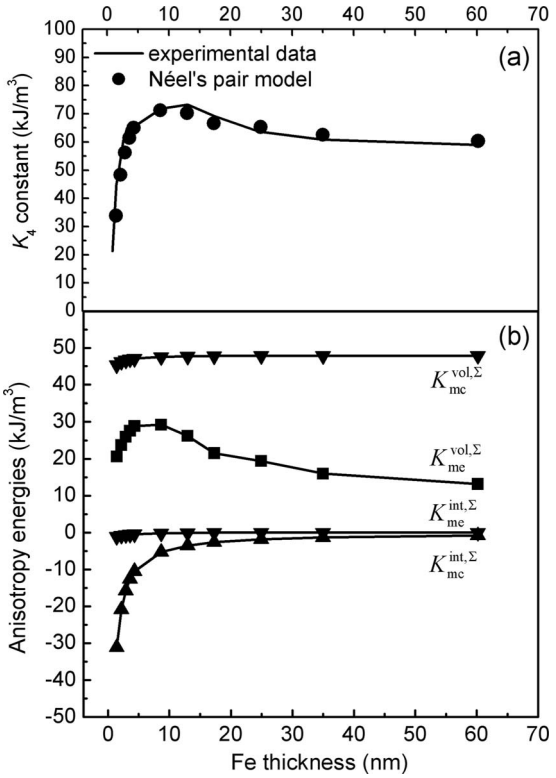

FIG. 7. (a) Thickness dependence of the constant K_4 experimentally determined (continuous line) compared with the curve calculated by means of the Néel's pair model (closed circles). (b) Contribution of each anisotropy energy to the in-plane fourfold magnetic anisotropy as a function of the iron thickness.

Concerning the volume terms, in Fig. 7(b) we observe that the magnetocrystalline anisotropy term is essentially constant on the whole range of Fe coverage, while the magnetoelastic anisotropy term ($K_{\mathrm{me}}^{\mathrm{vol},\Sigma}$) shows a nonmonotonous behavior. Note that the bulk magnetoelastic anisotropy induced by the in-plane tensile biaxial strain favors the ⟨100⟩ directions as the easy axis. Actually as discussed in Sec. III A, there is an increase in the stress-free lattice parameter of iron caused by the incorporation of In atoms into substitutional sites of the Fe lattice in the first planes above the $Fe/Al_{0.48}In_{0.52}As$ interface for the lower Fe coverage ($t_{\mathrm{Fe}}\leq1.5$ nm) where the film is pseudomorphous. The lattice distortions induced by the lattice mismatch with the substrate are therefore strongly reduced when compared with what is expected for pure iron. Then, when increasing the Fe coverage, as the In concentration profile above the $Fe/Al_{0.48}In_{0.52}As$ interface drops exponentially through the film thickness, the mean value of the in-plane lattice strain increases. As a result, the magnetoelastic anisotropy energy also increases. Finally, for a thickness higher than 4.4 nm a

stress relaxation mechanism takes place leading to a progressive diminution of the $K_{me}^{vol,\Sigma}$ value with the Fe coverage. Note that the diminution of the number of the NN and NNN Fe-Fe pairs caused by the presence of foreign species near the $Fe/Al_{0.48}In_{0.52}As$ interface induces a slight reduction in the strength of the magnetic anisotropy energy compared to that of a pure Fe film. This effect, however, is much weaker than the changes due to the magnetoelastic coupling.

Our analysis therefore shows that the dominant energies that drive the change in the K_4 constant with the iron thickness in Fig. 7(a) are the surface/interface magnetocrystalline anisotropy energy and the bulk magnetoelastic anisotropy energy: the surface magnetoelastic coupling effect seems to play a secondary role. It is interesting to note that the surface anisotropy energies are negative and below a critical Fe thickness ($t_{Fe}^{crit} \approx 0.7$ nm) the in-plane fourfold easy axis of the Fe layers must be along the $\langle 110 \rangle$ directions. Such a behavior with similar values for t_{Fe}^{crit} has already been observed in Au/Fe/Au(001), Ag/Fe/Ag(001), and Au/Fe/GaAs(001) systems[24,43] as well as in Fe/V(001) superlattices.[48] The calculation of the K_{mc}^{int} term for a pure bcc Fe(001) film yields a value of $-(2.4 \pm 0.9) \times 10^{-5}$ J/m^2 that is close to the experimentally determined in-plane fourth-order surface anisotropy constant for systems such as Au/Fe/Au(001),[42] Ag/Fe/Ag(001),[43] Au/Fe/GaAs(001),[35] Cu/Fe/GaAs(001),[44] or Au/Fe/ZnSe(001).[36] This confirms that the approximation that consists of neglecting the interaction energies between Fe and nonmagnetic atoms is reasonable for the surface and bulk Fe atoms and shows that the in-plane fourfold surface anisotropy in these systems is dominated by the surface magnetocrystalline anisotropy.

In our approach, the surface roughness in the iron films was not taken into account. Yet, the roughness influences the magnetic properties (anisotropy, coercitivity, etc.) of the magnetic films. For example an in-plane demagnetizing field caused by a magnetic charge distribution at the film surface can be produced by an isotropic surface roughness in magnetic films where the magnetization is in-plane and homogeneous.[49,50] At this stage we are not able to estimate the impact of these effects on the magnetic anisotropy properties because we do not have enough information on the surface/interface morphology. We know from our scanning tunneling microscopy images that for an uncapped layer of 1.5 nm Fe thickness the root-mean-square roughness amplitude value of the film surface is of 0.3 nm over 100×100 nm^2 surfaces with a lateral correlation length of 4 nm. This roughness is similar to what is observed with Fe/GaAs(001) system. Obviously, this surface roughness must induce effects that can distort our interpretations about magnetic anisotropies. However, the in-plane demagnetizing factor caused by surface roughness decreases with film thickness under certain conditions as was discussed in Refs. 49 and 51. Besides, the Néel's pair model allowed us to well reproduce the thickness dependence of K_4 on the whole range of Fe coverage with films in which both the surface and the interface were assumed perfectly plane. In particular the interaction parameters deduced from the analysis of experimental data through the Néel's pair model are essentially constant (see Fig. 6) between 4.4 and 60 nm. This suggests that in our case the effects associated to the surface roughness do not play a major role. They can however lead to small corrections on the values of $nq(r_1)$ and $nq(r_2)$ that we have determined. Note also that the in-plane magnetic anisotropy associated with surface defects such as steps or kinks are not taken into account. Yet calculations by means of the pair interaction model show that these defects also influence the in-plane surface magnetic anisotropy. Hence, it should be interesting to study in detail the roughness of the buried interfaces ($Fe/Al_{0.48}In_{0.52}As$ and Au/Fe) using techniques such as the grazing incidence x-ray scattering or resonant magnetic x-ray scattering[52] in order to estimate the influence of the surface roughness on the magnetic energy of the Fe films.

IV. CONCLUSION

Using XRD and MOKE techniques we have studied the structural and magnetic anisotropy properties of epitaxial Fe films between 0.9 and 60 nm deposited on $Al_{0.48}In_{0.52}As(001)$ surfaces. We observe that the in-plane magnetic anisotropy is a superposition of uniaxial and biaxial contributions with magnetization easy axes along the [110] and $\langle 100 \rangle$ directions, respectively. Our results suggest that the uniaxial anisotropy, whose strength decreases with the iron thickness, finds its origin in anisotropic bonding at the $Fe/Al_{0.48}In_{0.52}As$ interface. A remarkable feature in our study is the nonmonotonous change in the fourth-order anisotropy constant (K_4) when increasing the iron coverage. This behavior can be explained by means of the Néel's pair model in which the strain effects as well as the presence of foreign species located in the substitutional sites of the Fe lattice close to the $Fe/Al_{0.48}In_{0.52}As$ are taken into account. The expansion of the interaction energy to the first order in strains is sufficient to well reproduce the experimental data and in this work we have determined values for the high-order Néel parameters. From our analysis through the Néel's pair model, we find that the change in the K_4 value with the iron coverage is mainly caused by both the fourfold surface magnetocrystalline anisotropy whose contribution to the total magnetic anisotropy energy is inversely proportional to the Fe thickness, and by the lattice misfit strain effects in the film through the bulk magnetoelastic coupling.

ACKNOWLEDGMENTS

The authors thank G. Gewinner for fruitful discussions, M. Vallet for the MOKE instrumental developments, L. Frein and A. Le Pottier for technical support and the Laboratoire de Chimie du Solide et Inorganique Moléculaire of University of Rennes1 for providing access to XRD experiments. This work was supported by the French ANR Program Nanosciences and Nanotechonology (PNANO).

APPENDIX

In order to include the effects relative to film inhomogeneities in the Néel's pair model we have expressed the in-plane fourth-order anisotropy constant K_4 under the form

$$K_4 = \sum_{j=1}^{N} \frac{1}{N}(K_{4,\mathrm{mc}}^{\mathrm{vol},j} + K_{4,\mathrm{me}}^{\mathrm{vol},j}) + \frac{K_{4,\mathrm{mc}}^{\mathrm{int},1} + K_{4,\mathrm{me}}^{\mathrm{int},1}}{t_{\mathrm{Fe}}} + \frac{K_{4,\mathrm{mc}}^{\mathrm{int},N} + K_{4,\mathrm{me}}^{\mathrm{int},N}}{t_{\mathrm{Fe}}}. \tag{A1}$$

In this relation the various terms are deduced from Eqs. (12)–(15) and are established by neglecting the pair interaction energies between Fe and nonmagnetic atoms (Al, As or In) and considering a bcc Fe-based disordered alloy. In such an alloy, the number of Fe-Fe pairs is proportional to the square of the Fe atomic concentration.[9] Hence, Eqs. (12)–(15) remain valid provided the interaction parameters are multiplied by $C_{\mathrm{Fe},j}^2$. Note however that the cubic anisotropy constant deduced from the MOKE measurements is given in joule per unit volume of iron; consequently the different terms can be written as follows:

$$K_{4,\mathrm{me}}^{\mathrm{vol},j} = nC_{\mathrm{Fe},j}\left\{\left[\left(\frac{32}{27}r_{1,j} - 2r_{2,j}\right)s + \frac{64}{27}q(r_{1,j})\right]e_{\parallel,j} + \left[\frac{16}{27}r_{1,j}s - \frac{64}{27}q(r_{1,j})\right]e_{\perp,j}\right\}, \tag{A2}$$

$$K_{4,\mathrm{mc}}^{\mathrm{vol},j} = nC_{\mathrm{Fe},j}\left[\frac{16}{9}q(r_{1,j}) - 2q(r_{2,j})\right], \tag{A3}$$

$$K_{4,\mathrm{me}}^{\mathrm{int},j} = na_{\mathrm{Fe}}C_{\mathrm{Fe},j}\left\{\left[-\frac{8}{27}r_{1,j}s - \frac{16}{27}q(r_{1,j})\right]e_{\parallel,j} + \left[-\frac{4}{27}r_{1,j}s + \frac{16}{27}q(r_{1,j})\right]e_{\perp,j}\right\}, \tag{A4}$$

and

$$K_{4,\mathrm{mc}}^{\mathrm{int},j} = na_{\mathrm{Fe}}C_{\mathrm{Fe},j}\left[-\frac{4}{9}q(r_{1,j})\right]. \tag{A5}$$

Using the same notations and approximations as in Sec. III A, we have simply included the strain inhomogeneity in the Néel's pair model by replacing in Eqs. (12) and (13), $e_{\parallel}$ and $e_{\perp}$ by $e_{\parallel,j}=(a_{\parallel}-a_{0,j})/a_{0,j}$ and $e_{\perp,j}=-2e_{\parallel,j}C_{12}/C_{11}$, respectively. The in-plane lattice parameter $a_{\parallel}$, deduced from XRD measurements, is assumed homogeneous across the film and $a_{0,j}=a_{\mathrm{Fe}}(1-C_{\mathrm{In},j})+a_{\mathrm{In}}C_{\mathrm{In},j}$. In the same manner the radii r_1 and r_2 are replaced in Eqs. (12)–(15), respectively, by $r_{1,j}$ and $r_{2,j}$: $r_{1,j}=\sqrt{3}a_{0,j}/2$ and $r_{2,j}=a_{0,j}$. Finally, for simplicity, we have made the following approximations: $q(r_{1,j}) \approx q(r_1)+s(r_{1,j}-r_1)$ and $q(r_{2,j}) \approx q(r_1)+s(r_{2,j}-r_1)$. Note that the influence of the other species (Al and As) incorporated into Fe lattice is neglected because their atomic volume in a bcc structure is very close to that of bcc iron.

[1] C. A. F. Vaz, J. A. C. Bland, and G. Lauhoff, Rep. Prog. Phys. **71**, 056601 (2008).
[2] D. Sander, Rep. Prog. Phys. **62**, 809 (1999).
[3] D. Sander, A. Enders, and J. Kirschner, J. Magn. Magn. Mater. **200**, 439 (1999).
[4] K. Ha and R. C. O'Handley, J. Appl. Phys. **85**, 5282 (1999).
[5] M. Komelj and M. Fähnle, Phys. Rev. B **65**, 212410 (2002).
[6] A. Broddefalk, P. Nordblad, P. Blomquist, P. Isberg, R. Wäppling, O. Le Bacq, and O. Eriksson, J. Magn. Magn. Mater. **241**, 260 (2002).
[7] P. Bertoncini, P. Wetzel, D. Berling, A. Mehdaoui, B. Loegel, G. Gewinner, R. Poinsot, and V. Pierron-Bohnes, J. Magn. Magn. Mater. **237**, 191 (2001).
[8] N. Tournerie, P. Schieffer, B. Lépine, C. Lallaizon, and G. Jézéquel, IEEE Trans. Magn. **41**, 3322 (2005).
[9] L. Néel, J. Phys. Radium **15**, 225 (1954).
[10] Etienne du Trémolet de Lacheisserie, *Magnetostriction: Theory and Applications of Magnetoelasticity* (CRC, Boca Raton, FL, 1993), p. 61, p. 231.
[11] E. du Trémolet de Lacheisserie and O. F. K. Mc Grath, J. Magn. Magn. Mater. **147**, 160 (1995).
[12] Y. T. Millev, R. Skomski, and J. Kirschner, Phys. Rev. B **58**, 6305 (1998).
[13] E. du Trémolet de Lacheisserie, J. Phys. (France) **29**, 1066 (1968).
[14] D. S. Chuang, C. A. Ballentine, and R. C. O'Handley, Phys. Rev. B **49**, 15084 (1994).
[15] G. Bayreuther, M. Dumm, B. Uhl, R. Meier, and W. Kipferl, J. Appl. Phys. **93**, 8230 (2003).
[16] P. Schieffer, N. Tournerie, B. Lépine, C. Lallaizon, A. Guivarc'h, and G. Jézéquel, J. Phys. IV **132**, 225 (2006).
[17] D. H. Chung and W. R. Buessem, in *Anisotropy in Single Crystal Refractory Compound*, edited by F. W. Vahldiek and S. A. Mersol (Plenum, New York, 1968), Vol. 2, p. 217.
[18] N. Tournerie, Ph.D. thesis, Rennes 1 University, 2005.
[19] O. Thomas, P. Müller, P. Gergaud, and S. Labat, J. Appl. Phys. **91**, 2951 (2002).
[20] P. Schieffer, A. Guivarc'h, C. Lallaizon, B. Lépine, D. Sébilleau, P. Turban, and G. Jézéquel, Appl. Phys. Lett. **89**, 161923 (2006).
[21] Sang H. Yang, Michael J. Mehl, and D. A. Papaconstantopoulos, Phys. Rev. B **57**, R2013 (1998).
[22] V. Blum, L. Hammer, W. Meier, K. Heinz, M. Schmid, E. Lundgren, and P. Varga, Surf. Sci. **474**, 81 (2001).
[23] G. Häg, Nova Acta Regiae Soc. Sci. Ups. **7**, 44 (1929).
[24] R. Moosbühler, F. Bensch, M. Dumm, and G. Bayreuther, J. Appl. Phys. **91**, 8757 (2002).
[25] O. Thomas, Q. Shen, P. Schieffer, N. Tournerie, and B. Lépine, Phys. Rev. Lett. **90**, 017205 (2003).
[26] M. Dumm, M. Zölfl, R. Moosbühler, M. Brockmann, T. Schmidt, and G. Bayreuther, J. Appl. Phys. **87**, 5457 (2000).
[27] C. Daboo, R. J. Hicken, E. Gu, M. Gester, S. J. Gray, D. E. P. Eley, E. Ahmad, J. A. C. Bland, R. Ploessl, and J. N. Chapman, Phys. Rev. B **51**, 15964 (1995).
[28] K. Postava, H. Jaffrès, A. Schuhl, F. Nguyen Van Dau, M. Goiran, and A. R. Fert, J. Magn. Magn. Mater. **172**, 199 (1997).
[29] R. M. Osgood III, S. D. Bader, B. M. Clemens, R. L. White, and H. Matsuyama, J. Magn. Magn. Mater. **182**, 297 (1998).
[30] R. Mattheis and G. Quednau, J. Magn. Magn. Mater. **205**, 143 (1999).

[31] D. Berling, S. Zabrocki, R. Stephan, G. Garreau, J. L. Bubendorff, A. Mehdaoui, D. Bolmont, P. Wetzel, C. Pirri, and G. Gewinner, J. Magn. Magn. Mater. **297**, 118 (2006).
[32] K. Postava, D. Hrabovský, J. Pištora, A. R. Fert, Š. Višňovský, and T. Yamaguchi, J. Appl. Phys. **91**, 7293 (2002).
[33] K. Postava, J. Pištora, D. Ciprian, D. Hrabovský, M. Lesňák, and A. R. Fert, Proc. SPIE **3820**, 412 (1999).
[34] U. Ebels, M. Gester, C. Daboo, and J. A. C. Bland, Thin Solid Films **275**, 172 (1996).
[35] S. McPhail, C. M. Gürtler, F. Montaigne, Y. B. Xu, M. Tselepi, and J. A. C. Bland, Phys. Rev. B **67**, 024409 (2003).
[36] E. Reiger, E. Reinwald, G. Garreau, M. Ernst, M. Zölfl, F. Bensch, S. Bauer, H. Preis, and G. Bayreuther, J. Appl. Phys. **87**, 5923 (2000).
[37] M. Košuth, V. Popescu, H. Ebert, and G. Bayreuther, Europhys. Lett. **72**, 816 (2005).
[38] E. Sjöstedt, L. Nordström, F. Gustavsson, and O. Eriksson, Phys. Rev. Lett. **89**, 267203 (2002).
[39] E. du Trémolet de Lacheisserie, Ann. Phys. (N.Y.) **5**, 267 (1970).
[40] R. Gersdorf, Physica (Amsterdam) **34**, 254 (1967).
[41] E. du Trémolet de Lacheisserie, Phys. Rev. B **51**, 15925 (1995).
[42] M. Brockmann, S. Miethaner, R. Onderka, M. Köhler, F. Himmelhuber, H. Regensburger, F. Bensch, T. Schweinböck, and G. Bayreuther, J. Appl. Phys. **81**, 5047 (1997).
[43] T. Leeb, M. Brockmann, F. Bensch, S. Miethaner, and G. Bayreuther, J. Appl. Phys. **85**, 4964 (1999).
[44] T. L. Monchesky, B. Heinrich, R. Urban, K. Myrtle, M. Klaua, and J. Kirschner, Phys. Rev. B **60**, 10242 (1999).
[45] E. G. Moroni, W. Wolf, J. Hafner, and R. Podloucky, Phys. Rev. B **59**, 12860 (1999).
[46] V. A. Niculescu, T. J. Burch, and J. I. Budnick, J. Magn. Magn. Mater. **39**, 223 (1983).
[47] V. Blum, Ch. Rath, S. Müller, L. Hammer, K. Heinz, J. M. García, J. E. Ortega, J. E. Prieto, O. S. Hernán, J. M. Gallego, A. L. Vázquez de Parga, and R. Miranda, Phys. Rev. B **59**, 15966 (1999).
[48] A. N. Anisimov, W. Platow, P. Poulopoulos, W. Wisny, M. Farle, K. Baberschke, P. Isberg, B. Hjövarsson, and R. Wäppling, J. Phys.: Condens. Matter **9**, 10581 (1997).
[49] Y.-P. Zhao, G. Palasantzas, G.-C. Wang, and J. Th. M. De Hosson, Phys. Rev. B **60**, 1216 (1999).
[50] Q. Jiang, H.-N. Yang, and G.-C. Wang, Surf. Sci. **373**, 181 (1997).
[51] E. Schlömann, J. Appl. Phys. **41**, 1617 (1970).
[52] R. M. Osgood III, S. K. Sinha, J. W. Freeland, Y. U. Idzerda, and S. D. Bader, J. Appl. Phys. **85**, 4619 (1999).